• Basic Research •

Glucocorticoid-induced RPE injury in ARPE-19 cells: association with excessive autophagy and AMPK/mTOR signaling

Wen-Xue Guan[1,2,3], *Yue Guo*[1,2,3], *Si-Tong Chen*[1,2,3], *Zhi-Ming Liu*[1,2,3], *Yao-Yao Sun*[1,2,3], *Ming-Wei Zhao*[1,2,3]

[1]Department of Ophthalmology, Peking University People's Hospital, Beijing 100044, China
[2]Beijing Key Laboratory of Ocular Disease and Optometry Science, Peking University People's Hospital, Beijing 100044, China
[3]College of Optometry, Peking University Health Science Center, Beijing 100044, China
Co-first Authors: Wen-Xue Guan and Yue Guo
Correspondence to: Ming-Wei Zhao. Department of Ophthalmology, Peking University People's Hospital; Beijing Key Laboratory of Ocular Disease and Optometry Science; College of Optometry, Peking University Health Science Center, Xizhimen South Street 11, Xicheng District, Beijing 100044, China. zhaomingwei64@163.com
Received: 2025-04-14 Accepted: 2026-06-12

Abstract

● **AIM:** To investigate whether excessive glucocorticoid (GC) exposure disrupts retinal pigment epithelial (RPE) homeostasis through glucocorticoid receptor (GR)-dependent autophagy hyperactivation.

● **METHODS:** Human retinal pigment epithelial cell line (ARPE-19 cells) were exposed to GC (0–100 μmol/L, 48h). GR subcellular localization was analyzed *via* mitochondrial fractionation and immunofluorescence. Functional assessments included barrier integrity [zonula occludens-1 (ZO-1) immunostaining], phagocytic capacity (FluoSpheres™-labeled photoreceptor outer segment uptake), and ultrastructural analysis (transmission electron microscopy, TEM). Autophagic flux was quantified using mCherry-green fluorescent protein-microtubule-associated protein 1A/1B-light chain 3 (LC3) B reporters. Molecular mechanisms were probed through AMP-activated protein kinase (AMPK)/mammalian target of rapamycin (mTOR) pathway activity and autophagic flux assessed by LC3-II levels. GR dependency was confirmed using the antagonist RU486, and cell-type specificity was assessed using mouse photoreceptor (661W) cells.

● **RESULTS:** GC induced GR upregulation and mitochondrial translocation in a dose- and time-dependent manner, correlating with pathological autophagy activation. Key findings included: 1) tight junction disruption, evidenced by ZO-1 fragmentation, 2) reduction in phagocytic uptake efficiency, 3) mitochondrial shrinkage and autolysosome accumulation (TEM), 4) altered AMPK/mTOR signaling (p-AMPK up, p-mTOR down) associated with autophagosome formation, 5) elevated LC3-II levels confirming excessive autophagic flux. Critically, all GC-induced effects, including GR upregulation, signaling changes, and increased autophagy, were abolished by GR antagonism with RU486.

● **CONCLUSION:** This study shows that GR-dependent GC exposure induces autophagic flux with ultrastructural evidence suggestive of mitochondria-targeted autophagy and alters AMPK/mTOR signaling, correlating with RPE barrier collapse and phagocytic failure, a possible link to steroid-associated central serous chorioretinopathy (CSC).

● **KEYWORDS:** glucocorticoid; autophagy; retinal pigment epithelial cells; central serous chorioretinopathy; AMPK/mTOR

DOI:10.18240/ijo.2026.09.01

Citation: Guan WX, Guo Y, Chen ST, Liu ZM, Sun YY, Zhao MW. Glucocorticoid-induced RPE injury in ARPE-19 cells: association with excessive autophagy and AMPK/mTOR signaling. *Int J Ophthalmol* 2026;19(9):1657-1666

INTRODUCTION

Central serous chorioretinopathy (CSC) is an idiopathic disease characterized by serous retinal detachment resulting from choroidal vascular hyperpermeability and secondary leakage of the retinal pigment epithelium (RPE)[1]. It represents a leading cause of vision-threatening retinopathy, after age-related macular degeneration, diabetic retinopathy, and branch retinal vein occlusion, with a significant male predominance (annual incidence: 9.9 *vs* 1.7 per 100 000)[2].

Typical clinical manifestations include acute-onset blurred vision, metamorphopsia, micropsia, and dyschromatopsia. While spontaneous resolution occurs in some patients, chronic or recurrent CSC can cause permanent visual impairment due to irreversible damage to the RPE and photoreceptors[3-4].

Current mechanistic hypotheses posit that CSC arises primarily from choroidal vascular dysfunction, which secondarily disrupts RPE homeostasis. Strategically positioned between the photoreceptors and choriocapillaris, the RPE performs energy-demanding functions, such as phagocytosing photoreceptor outer segments, which are supported by an extensive mitochondrial network[5]. Nevertheless, the molecular drivers linking these structural and metabolic vulnerabilities to CSC progression remain poorly understood. Several risk factors have been identified for CSC, including psychological stress, corticosteroid exposure, endocrinopathies, pregnancy, and psychotropic medication use. Among these, glucocorticoid (GC), a subclass of corticosteroids, have emerged as a principal research focus[5-6]. Both endogenous hypercortisolism (*e.g.*, Cushing's syndrome) and exogenous GC exposure exhibit strong epidemiological associations with CSC development[7-8]. Recent mechanistic studies delineate how GC concurrently disrupts ocular homeostasis by inducing choroidal nervous system dysregulation and impairing ion and water transport across the RPE[9-10]. These molecular alterations likely contribute to RPE barrier dysfunction, thereby providing a plausible link between GC excess and CSC pathogenesis.

Autophagy is an evolutionarily conserved lysosomal degradation pathway that maintains cellular homeostasis by selectively eliminating damaged organelles and protein aggregates[11]. While physiologically cytoprotective, pathological hyperactivation of this process may trigger autophagic cell death[12-13]. As a specialized form of autophagy, mitophagy specifically targets dysfunctional mitochondria for lysosomal degradation, thereby maintaining mitochondrial quality control[14]. Notably, GC has been reported to upregulate both autophagy and mitophagy[15-16]. Furthermore, glucocorticoid receptors (GR) can translocate into mitochondria and directly regulate mitochondrial gene transcription and metabolism, suggesting a potential mechanism for GC-induced mitophagy[17]. Despite these advances, the pathophysiological relationship between GC-driven autophagic activity involving mitochondria and RPE dysfunction in CSC remains unexplored.

Previous studies have implicated dysregulated autophagy, including mitophagy, in the pathogenesis of multiple ophthalmologic disorders, including glaucoma, diabetic retinopathy, and age-related macular degeneration[18-20]. Based on this evidence, we hypothesize that excessive GC exposure disrupts RPE homeostasis through GR-mediated hyperactivation of autophagy, accompanied by ultrastructural evidence of mitochondrial targeting.

MATERIALS AND METHODS

Cell Culture and Treatment The human RPE cell line human retinal pigment epithelial cell line 19 (ARPE-19) was obtained from the Cell Bank of the Chinese Academy of Sciences (Shanghai, China). The 661W cell line was obtained from an internal laboratory repository and maintained in our facility. Cells were cultured in Dulbecco's modified eagle medium/nutrient mixture F-12 (Gibco, Carlsbad, CA, USA) supplemented with 10% heat-inactivated fetal bovine serum and 1% penicillin-streptomycin. Cells were maintained at 37℃ in a humidified atmosphere with 5% CO_2. Cell line authentication was performed by short tandem repeat profiling, with regular mycoplasma contamination screening. At approximately 90% confluence, cells were dissociated with 0.25% trypsin and seeded into six-well plates. At 70%–80% confluence, cells were treated with GC (C104537, Aladdin Reagent, Shanghai, China) at concentrations of 0, 500 nmol/L, 1, 10, and 100 μmol/L. Following 48-hour stimulation, cells were harvested for functional and signaling pathway analyses. For GR inhibition experiments, cells were pre-treated with the specific GR antagonist Mifepristone (RU486; Sigma-Aldrich, M8046) at a concentration of 10 μmol/L for 1h prior to GC exposure.

Mitochondria Isolation To assess mitochondrial functional changes following GC treatment, mitochondria were isolated from ARPE-19 cells using the mitochondria isolation kit for cultured cells (Beyotime Biotechnology, C3601). Briefly, cells were rinsed twice with ice-cold phosphate-buffered saline (PBS), harvested by trypsinization, and pelleted by centrifugation at 1000×g for 5min at 4℃. The pellet was resuspended in 1 mL mitochondrial isolation buffer and homogenized with 30 strokes in a pre-chilled Dounce homogenizer. The homogenate was centrifuged at 800×g for 10min at 4℃ to remove nuclei and cellular debris. The supernatant was then centrifuged at 10 000×g for 10min at 4℃ to obtain the mitochondrial fraction. The mitochondrial pellet was washed twice with isolation buffer and resuspended in storage buffer. Purity was verified through Western blot analysis using mitochondrial marker cytochrome c oxidase subunit IV (COX IV) and cytosolic marker glyceraldehyde 3-phosphate dehydrogenase (GAPDH).

MitoTracker Staining and Immunofluorescence Analysis Mitochondrial morphology was assessed using MitoTracker™ Red CMXRos (M7512, Thermo Fisher Scientific, USA). Briefly, treated cells were washed three times with PBS and incubated with 200 nmol/L MitoTracker in serum-free medium at 37℃ for 30min protected from light. Following live-cell staining, cells were fixed with 4% paraformaldehyde (PFA)

for 15min at room temperature (RT), then permeabilized with 0.25% Triton X-100 for 10min at RT. Non-specific binding was blocked with 5% normal donkey serum for 1h at RT. For immunostaining, cells were incubated overnight at 4℃ with primary antibodies. For GR detection, rabbit monoclonal anti-GR (1:500; Clone D6H2L; Cell Signaling Technology, 12041T) was used. For zonula occludens-1 (ZO-1) detection, rabbit polyclonal anti-ZO-1 (1:500; 61-7300, Thermo Fisher Scientific) was used on separate samples. After washing, all samples were incubated with Alexa Fluor™ 488-conjugated goat anti-rabbit IgG (1:1000; A11008, Thermo Fisher Scientific) for 1h at RT in darkness. Nuclei were counterstained with 4,6-diamidino-2-phenylindole (DAPI; 1 μg/mL, D1306, Thermo Fisher Scientific) for 5min. Confocal imaging was performed using a Leica TCS SP8 WLL system. For each independent biological replicate (n=3), at least five random fields per condition were captured. GR-mitochondria colocalization and ZO-1 tight junction integrity was assessed qualitatively by visual inspection of representative images.

Phagocytosis Assay ARPE-19 cells were seeded on glass coverslips in 24-well plates and allowed to adhere for 24h. Following GC treatment, phagocytic activity was assessed using carboxylate-modified FluoSpheres™ (F8803, Thermo Fisher Scientific, USA). Fluorescent microspheres were suspended in complete medium at a final concentration of 2 μL/mL and then added to the cells for a 4-hour incubation at 37℃. Uninternalized beads were removed by three PBS washes (5min each). Cells were fixed with 4% PFA for 15min at RT, followed by cytoskeletal staining with Alexa Fluor™ 594 phalloidin (1:200; A12381, Thermo Fisher Scientific) for 1h at RT protected from light. Nuclei were counterstained with DAPI (1 μg/mL, 5min). Confocal imaging was performed using a Leica TCS SP8 WLL system. Representative images from three independent biological replicates are shown. All analyses were performed in a blinded manner (the investigator was unaware of treatment groups during image acquisition and analysis).

Transmission Electron Microscopy For ultrastructural analysis, control and GC-treated (1 μmol/L, 48h) ARPE-19 cells were processed as follows: primary fixation in 2.5% glutaraldehyde, followed by post-fixation with 1% osmium tetroxide. Samples were dehydrated through a graded series of ethanol and acetone and embedded in Epon resin. Ultrathin sections were prepared using a Leica EM UC7 ultramicrotome and doubly stained with uranyl acetate and lead citrate. Images were acquired using a JEOL JEM-F200 transmission electron microscope (TEM). From three independent replicates, at least 3 random fields per condition were examined in a blinded manner.

Autophagic Flux Measurement Autophagic flux was monitored using an adenovirus expressing mCherry-GFP-LC3B (C3011, Biotechnology, Shanghai, China). ARPE-19 cells were seeded in 24-well plates (1×10^5 cells/well) and infected with the adenovirus (multiplicity of infection, MOI=10) for 24h. Cells were then treated with 1 μmol/L or vehicle control for 48h. Autophagic flux was assessed by quantifying the fluorescence signals using a laser scanning confocal microscope (Leica TCS SP8). For each independent biological replicate (n=3), five random fields per condition were imaged. Autophagic flux was expressed as the red/green puncta ratio, calculated using a custom ImageJ macro on at least 15 cells. All analyses were performed in a blinded manner.

Western Blot Analysis ARPE-19 cells were lysed using radioimmunoprecipitation assay (RIPA) buffer supplemented with a protease and phosphatase inhibitor cocktail on ice for 20min. The lysates were centrifuged at 12 000×g for 15min at 4℃. The supernatants were carefully collected, and protein concentrations were measured using a bicinchoninic acid (BCA) assay kit (Beyotime, P0010) according to the manufacturer's instructions. Equal amounts of protein were denatured in sodium dodecyl sulfate (SDS) sample loading buffer (Beyotime, P0015F) at 95℃ for 5min. The denatured proteins were separated by electrophoresis on 4%–12% SDS-polyacrylamide gels. Following electrophoresis, the proteins were transferred onto a polyvinylidene fluoride (PVDF) membrane. The membranes were blocked with QuickBlock™ Western Blot Blocking Buffer (Beyotime, P0252) for 15min at RT, followed by incubation with primary antibodies diluted in QuickBlock™ primary antibody dilution buffer (Beyotime, P0256) overnight at 4℃. After washing, the membranes were incubated with fluorescent-dye-conjugated secondary antibodies for 1h at RT protected from light. The signals were detected using an Odyssey near-infrared imaging system (LI-COR). The following primary antibodies were used: β-actin (1:2000, #4967), GR (1:1000, #12041), COX IV (1:1000, #4850), AMP-activated protein kinase alpha (AMPKα; 1:1000, #2532), phospho-AMPK alpha (p-AMPKα; Thr172; 1:1000, #2535), mammalian target of rapamycin (mTOR; 1:1000, #2983), p-mTOR (Ser2448; 1:1000, #5536), LC3B (1:1000, #3868), all from Cell Signaling Technology.

Statistical Analysis Statistical analysis was performed using GraphPad Prism 9 software. Data are presented as mean±standard deviation (SD) from three independent biological replicates. Comparisons between two groups were analyzed using an unpaired Student's t-test. Comparisons among multiple groups were analyzed by one-way analysis of variance (ANOVA) followed by Dunnett's post hoc test for comparison against the control group. A P-value of less than 0.05 was considered statistically significant.

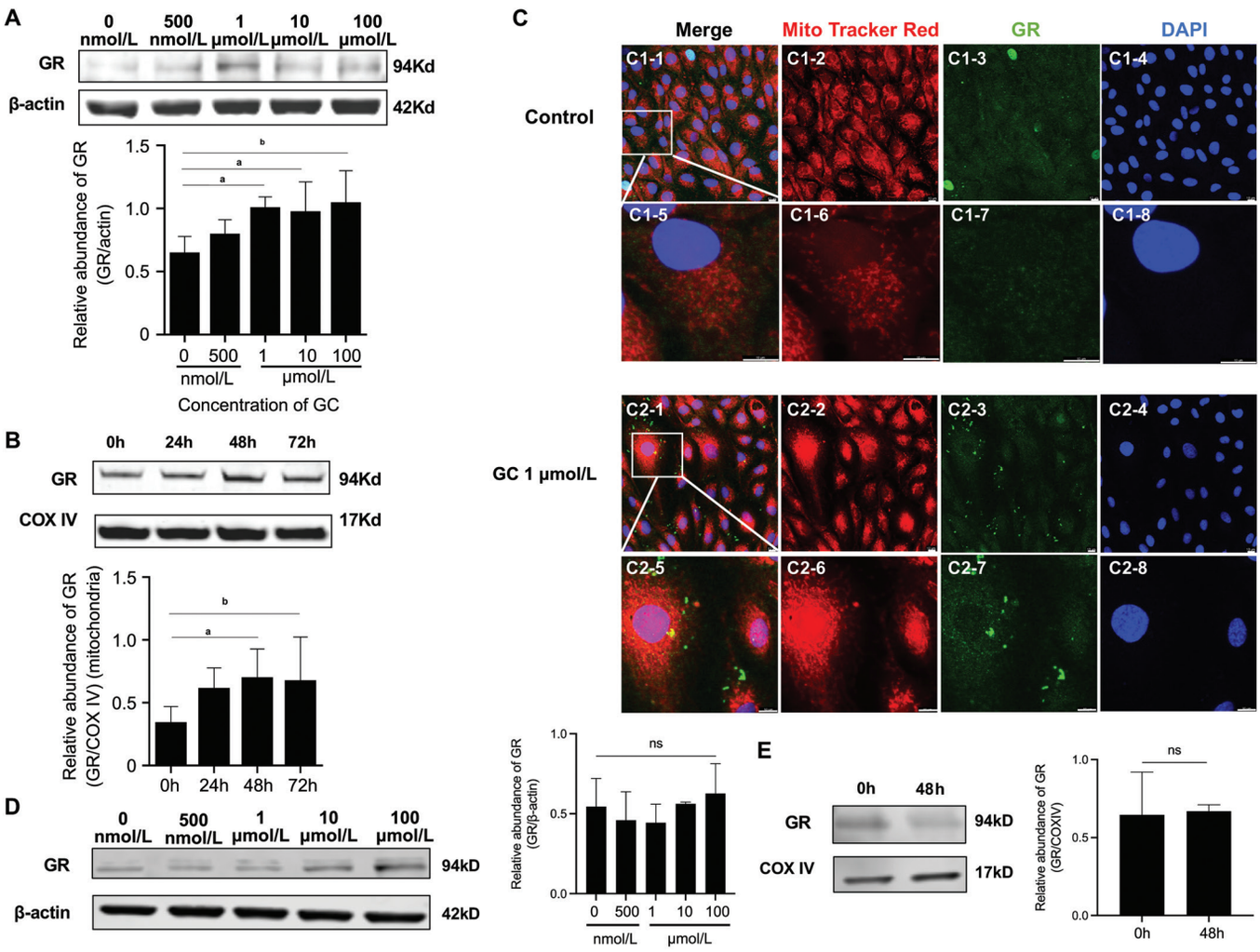

Figure 1 GC induces GR upregulation and mitochondrial translocation in a cell-type-specific manner A: ARPE-19 cells were treated with increasing concentrations of GC (0 to 100 μmol/L) for 48h. Representative Western blot and corresponding quantification show a dose-dependent upregulation of total GR protein. Data are mean±SD; $^{a}P<0.05$, $^{b}P<0.01$. B: Time-dependent GR translocation to mitochondria in ARPE-19 cells treated with 1 μmol/L GC. Mitochondrial fractions were isolated at the indicated times (0–72h). C: Immunofluorescence analysis of GR localization. Cells were stained for GR (green) and mitochondria (MitoTracker Red). Nuclei were counterstained with DAPI (blue). Scale bars: 10 μm. C1: In control (vehicle-treated) cells, GR displays a diffuse cytoplasmic distribution; C2: Treatment with 1 μmol/L GC for 48h induces pronounced clustering of GR around mitochondria, indicated by yellow signal in the merged panel. D: 661W cells were treated as in (A). Representative Western blot shows that GR protein levels remain unchanged across the tested concentration range. E: Mitochondrial fractions were isolated from 661W cells treated with 1 μmol/L GC or vehicle (control) for 48h. The absence of GR in mitochondrial fractions demonstrates the lack of translocation in this cell type. GC: Glucocorticoid; GR: Glucocorticoid receptor; ARPE-19: Human retinal pigment epithelial cell line 19; SD: Standard deviation; DAPI: 4′,6-diamidino-2-phenylindole; COX IV: Cytochrome C oxidase subunit IV; ns: Not significant.

RESULTS

GC Promotes GR Upregulation and Mitochondrial Translocation ARPE-19 cells were treated with a range of concentrations of GC concentrations (0, 500 nmol/L, 1, 10, 100 μmol/L) for 48h. Western blot analysis revealed a dose-dependent increase in total GR protein, with significant upregulation occurring at concentrations of 1 μmol/L and above (Figure 1A). To investigate the subcellular localization of GR, we performed subcellular fractionation and isolated mitochondrial proteins. Time-course experiments demonstrated progressive accumulation of GR in mitochondrial fractions following 1 μmol/L GC treatment (Figure 1B).

Immunofluorescence staining confirmed these findings, showing enhanced co-localization of GR with MitoTracker™-labeled mitochondria (Figure 1C). In control cells, GR was predominantly localized in the cytoplasm with minimal overlap with mitochondrial markers (Figure 1C). In contrast, treatment with GC exposure at 1 μmol/L induced pronounced clustering of GR around mitochondria, as evidenced by a substantial increase in co-localization signals (Figure 1C). To determine whether this response was cell type-specific, we examined GR expression in mouse photoreceptor-derived 661W cells.

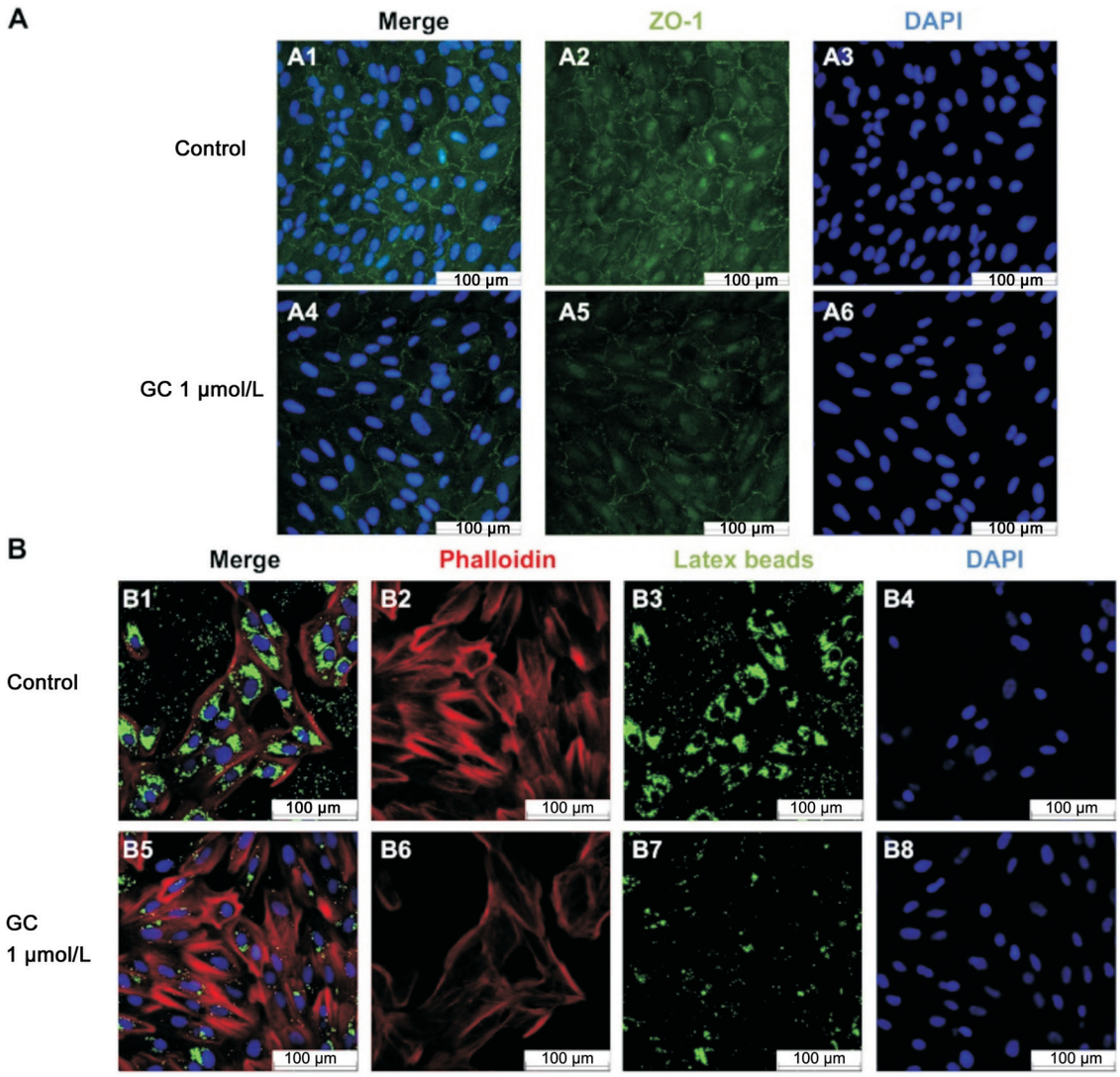

Figure 2 GC impairs tight junction integrity and phagocytic function in ARPE-19 cells A: Immunofluorescence staining of the tight junction protein ZO-1 (green). A1–A3: In control cells, ZO-1 forms a characteristic continuous, apical localization; A4–A6: Treatment with GC (1 μmol/L, 48h) disrupts the ZO-1 pattern, resulting in fragmentation and diminished fluorescence intensity. B: Phagocytic capacity assessed using fluorescent microspheres (green). B1–B4: Control cells display numerous internalized microspheres; B5–B8: GC-treated cells (1 μmol/L, 48h) exhibit both a reduction in internalized microspheres and aberrant extracellular aggregation of beads. Cells were co-stained for F-actin with phalloidin (red) and for nuclei with DAPI (blue). Scale bars: 100 μm. ARPE-19: Human retinal pigment epithelial cell line 19; GC: Glucocorticoid; ZO-1: Zonula occludens-1; DAPI: 4′,6-diamidino-2-phenylindole; F-actin: Filamentous actin.

In contrast to ARPE-19 cells, GR protein levels in 661W cells remained unaltered across the entire concentration range (0 to 100 μmol/L) of GC treatment (Figure 1D). Consistent with this, GC treatment did not promote GR translocation to mitochondria in 661W cells (Figure 1E). Together, these results identify the cell-type-specific upregulation and mitochondrial targeting of GR as a key amplifier of GC-induced toxicity, which may underlie the distinct susceptibility of RPE cells relative to other retinal cell types.

GC Compromises Tight Junction Integrity and Phagocytic Function in ARPE-19 Cells We next assessed whether GC exposure leads to functional impairments in ARPE-19 cells by examining tight junction integrity and phagocytic capacity. Immunofluorescence analysis of the tight junction protein ZO-1 revealed that GC treatment severely disrupted cellular architecture, as evidenced by a significant reduction in fluorescence intensity and the loss of the characteristic continuous, pericellular staining pattern (Figure 2A). Assessment of phagocytic function using fluorescent microspheres (FluoSpheres™) showed a significant reduction in the number of internalized beads in GC-treated cells compared with controls. Furthermore, we observed an abnormal accumulation of unengulfed microspheres at the cell junctions in the GC-treated group (Figure 2B). Together, these results demonstrate that GC exposure structurally compromises the outer blood-retinal barrier by disrupting tight junctions and

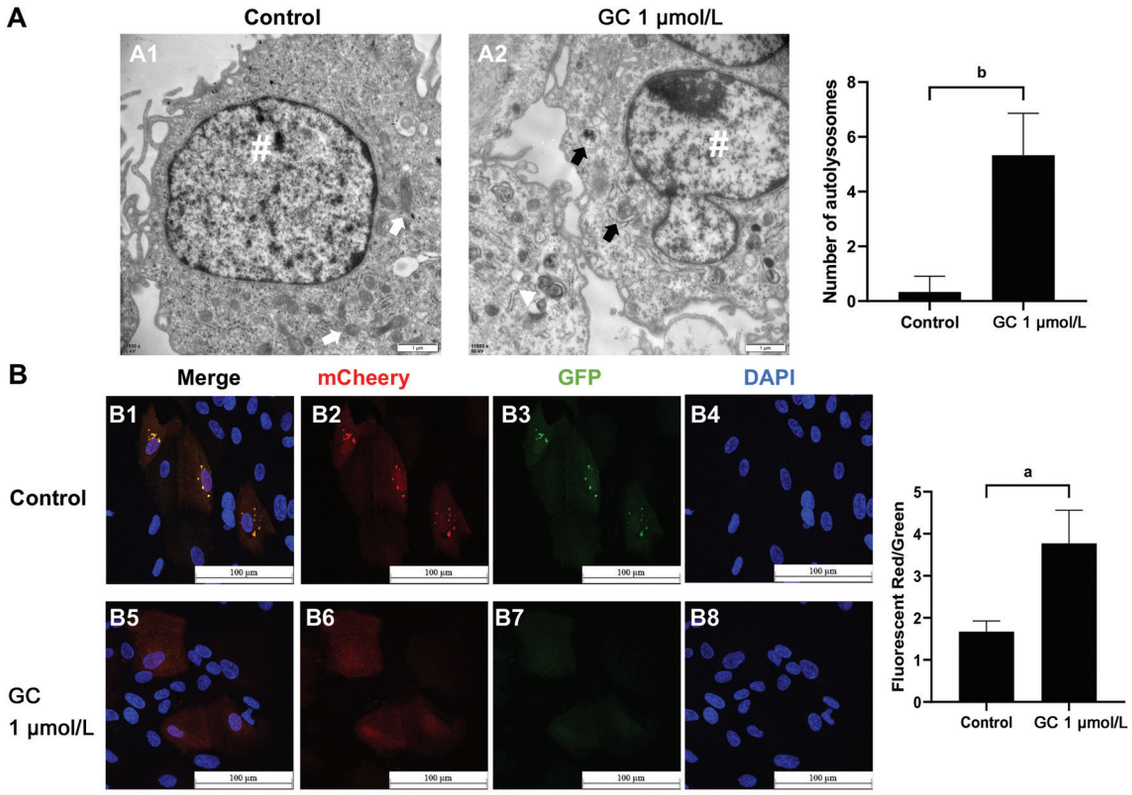

Figure 3 GC induces autophagic flux with ultrastructural evidence suggestive of mitochondria-targeted autophagy A: Transmission electron microscopy images of ARPE-19 cells. A1: Control cells showing mitochondria with normal cristae (white arrows); A2: Cells treated with GC (1 μmol/L, 48h) exhibit ultrastructural features suggestive of active autophagy involving mitochondria, including double-membrane phagophores (triangle) engulfing damaged mitochondria and autolysosomes containing partially degraded organelles (black arrows). The bar graph quantifies the number of autophagic vacuoles per cell profile. Data are presented as mean±SD; ^{b}P<0.01. Scale bars: 1 μm. B: Analysis of autophagic flux using the mCherry-GFP-LC3B reporter. B1–B4: In control cells, the presence of both GFP and mCherry signals results in yellow puncta, representing autophagosomes that have not yet fused with lysosomes; B5–B8: GC-treated cells (1 μmol/L, 48h) show a predominance of red puncta (mCherry-only signal), indicating the formation of acidified autolysosomes where GFP fluorescence is quenched. Nuclei are stained with DAPI (blue). The bar graph provides quantitative analysis of autophagic flux. Data are presented as mean±SD; ^{a}P<0.05. Scale bars: 100 μm. ARPE-19: Human retinal pigment epithelial cell line 19; SD: Standard deviation; GC: Glucocorticoid; LC3B: Microtubule-associated protein 1A/1B-light chain 3B; DAPI: 4′,6-diamidino-2-phenylindole; GFP: Green fluorescent protein.

concurrently impairs its physiological phagocytic function.

GC Induces Autophagic Flux with Ultrastructural Evidence Suggestive of Mitochondria-Targeted Autophagy TEM revealed progressive ultrastructural alterations in ARPE-19 cells treated with 1 μmol/L GC. Control cells exhibited normal mitochondrial morphology with intact cristae (Figure 3A, white arrows). In contrast, 48-hour GC treatment induced pronounced reorganization, characterized by double-membrane phagophores enveloping degenerating mitochondria (Figure 3A, triangle) and an accumulation of autolysosomes containing partially degraded organelles (Figure 3A, black arrows), features suggestive of mitochondria-targeted autophagy. To corroborate these findings, we monitored autophagic flux using the mCherry-GFP-LC3 reporter system. In this system, the GFP signal is quenched in the acidic environment of autolysosomes, while the mCherry signal remains stable. Consequently, a transition from yellow (GFP+ mCherry+) puncta in autophagosomes to red (mCherry+ only) puncta in autolysosomes indicates successful autophagic flux. GC-treated cells displayed an increase in red-only puncta compared to controls, indicating robust autophagic flux and completion (Figure 3B).

GC-Induced Autophagy Associated with AMPK/mTOR Pathway in ARPE-19 Cells To explore the signaling pathway potentially involved in GC-induced autophagy, we performed time-course Western blot analysis in ARPE-19 cells treated with 1 μmol/L GC (0–72h; Figure 4A, 4B). GC treatment resulted in a time-dependent upregulation of total GR protein. Concurrently, we observed changes in the AMPK/mTOR signaling axis, as evidenced by increased p-AMPK and decreased p-mTOR. Furthermore, the protein level of LC3-II was progressively increased, indicating accumulation of autophagosomes. These data suggest that the AMPK/mTOR axis is implicated in GC-induced autophagy in ARPE-19 cells.

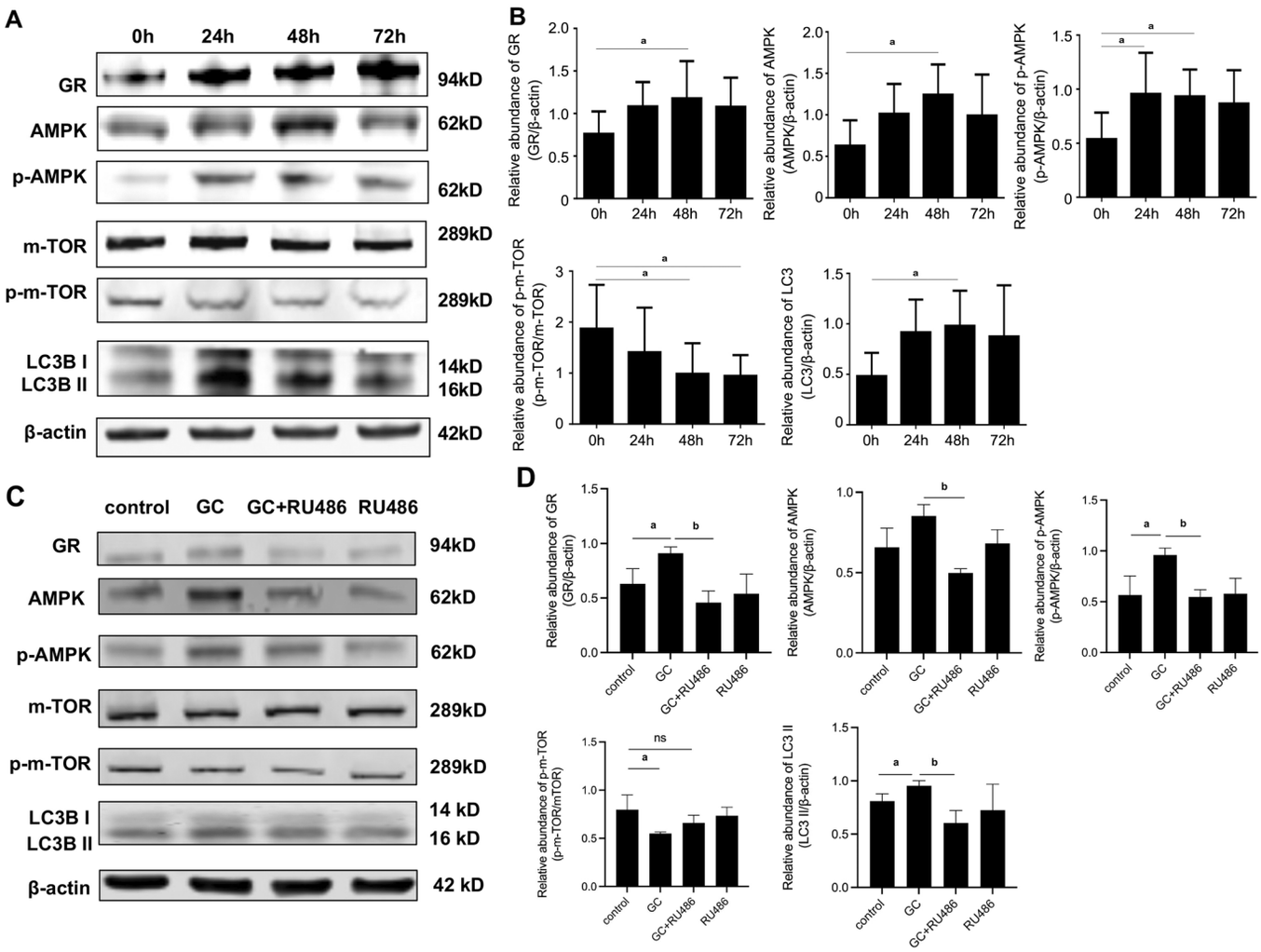

Figure 4 GC-induced autophagy is associated with AMPK/mTOR pathway in ARPE-19 cells A: Representative Western blots of key proteins in the mitophagy signaling pathway from ARPE-19 cells treated with 1 μmol/L GC for 24 to 72h. B: Densitometric quantification of A. C: RU486 inhibits GC-induced autophagy signaling. Cells were pre-treated with the GR antagonist RU486 (10 μmol/L) for 1h before and during a 48h co-exposure to 1 μmol/L GC. D: Densitometric quantification of C. All quantitative data are presented as mean±SD. $^{a}P<0.05$, $^{b}P<0.01$. GC: Glucocorticoid; AMPK: AMP-activated protein kinase; mTOR: Mammalian target of rapamycin; ARPE-19: Human retinal pigment epithelial cell line 19; LC3B: Microtubule-associated protein 1A/1B-light chain 3B; p-mTOR: Phospho-mTOR; p-AMPK: Phospho-AMPK; GR: Glucocorticoid receptor.

Pharmacological Inhibition of GR Abolishes GC-Induced Autophagy To assess the central role of GR, we pre-treated ARPE-19 cells with the GR antagonist mifepristone (RU486; 10 μmol/L) 1h before and during a 48h exposure to 1 μmol/L GC. RU486 co-treatment completely prevented the GC-induced upregulation of total GR protein (Figure 4C, 4D). Moreover, RU486 significantly attenuated the GC-mediated activation of the AMPK/mTOR pathway, reversing both the increase in p-AMPK and the decrease in p-mTOR. Consequently, the GC-induced increase in the LC3-II was also abolished by GR antagonism (Figure 4C, 4D). These results indicate that GR activation is required for initiating the downstream AMPK/mTOR signaling and pathological autophagy induced by GC. Based on these cumulative findings, we propose a model wherein GC triggers pathological autophagy in ARPE-19 cells in a GR-dependent manner, with the AMPK/mTOR axis implicated in this process (Figure 5)[21].

DISCUSSION

This *in vitro* study demonstrates that GC exposure leads to GR upregulation and its translocation to mitochondria in ARPE-19 cells. These events are associated with enhanced autophagic flux, as evidenced by LC3-II accumulation and ultrastructural features suggestive of mitochondria-targeted autophagy. Concomitant alterations in AMPK/mTOR signaling were observed. Functionally, this autophagic response correlated with RPE barrier disruption and impaired phagocytic capacity. Collectively, these findings provide *in vitro* mechanistic evidence linking GC exposure to RPE dysfunction, offering insight into its possible contribution to steroid-associated CSC.

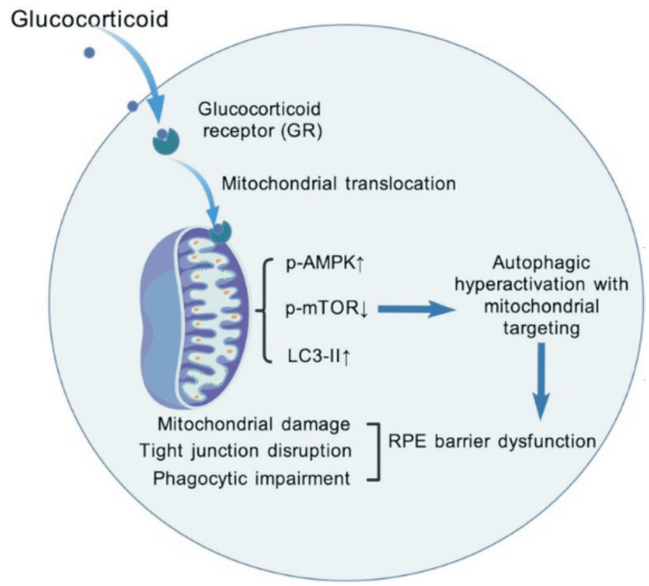

Figure 5 Proposed model of glucocorticoid-induced pathological autophagy in ARPE-19 cells[21] p-AMPK: Phospho-AMP-activated protein kinase; p-mTOR: Phospho-mammalian target of rapamycin; LC3: Microtubule-associated protein 1A/1B-light chain 3; ARPE-19: Human retinal pigment epithelial cell line 19; RPE: Retinal pigment epithelial. Created with BioGDP.com.

The biological effects of GC are primarily mediated through the GR, a ligand-activated member of the nuclear receptor superfamily that regulates diverse physiological processes including metabolism, development, and immune response[22]. In the unliganded states, GR predominantly localizes to the cytoplasm but undergoes rapid nuclear translocation upon ligand binding, where it can exert its actions mainly through genomic mechanisms[23]. While classical models emphasize nuclear GR signaling, accumulating evidence supports the hypothesis that mitochondrial GR directly regulates mitochondrial gene expression[17]. Moreover, mitochondrial GR translocation appears differentially regulated compared to nuclear GR trafficking, with studies suggesting its potential to induce apoptosis through independent or synergistic mechanisms[24].

Our findings suggest that GC triggers mitochondrial GR translocation along with receptor upregulation, which may contribute to RPE injury through mechanisms that are dependent on GR signaling. The GR dependency of this pathway is supported by our pharmacological inhibition experiments. Pretreatment with the specific GR antagonist RU486 blocked the GC-induced GR upregulation and mitochondrial translocation, as well as the accompanying changes in the AMPK/mTOR axis and the increase in autophagy. These results indicate that the observed pathological cascade is initiated through GR signaling, positioning GR as a key mediator of GC-induced RPE injury in our *in vitro* model.

Studies have established that GC exhibits biphasic regulation of neural plasticity: low-dose administration enhances neural plasticity and spatial memory performance, whereas chronic high-dose exposure induces inhibitory effects[17,25]. Correspondingly, GC demonstrates dual-phase modulation of mitochondrial dynamics in neurons. Physiological concentrations augment mitochondrial bioenergetic capacity (*e.g.*, increased ATP production and membrane potential), while sustained supraphysiological levels impair oxidative phosphorylation and promote reactive oxygen species overproduction[26]. These mitochondrial insults activate quality control pathways, triggering either repair or elimination *via* mitophagy.

Notably, Zhou *et al*[27] demonstrated that dexamethasone induces cardiomyocyte mitophagy through LC3-II recruitment to mitochondria and subsequent lysosomal engulfment. Similarly, GC-induced mitophagy has been implicated in osteocyte-mediated bone resorption *via* cathepsin K-dependent extracellular matrix degradation[28]. Extending this concept to the retina, a recent review by Chen *et al*[29] highlights that dysregulated mitophagy in the RPE is central to age-related macular degeneration, positioning RPE mitochondrial quality control failure as a key pathogenic mechanism across different retinal diseases. Consistent with these findings, our study revealed that GC administration induced ultrastructural mitochondrial pathology in RPE cells, characterized by double-membrane phagophores encapsulating degenerating mitochondria, autolysosomal accumulation, and elevated autophagic flux fluorescence. Taken together, these observations suggest that GC-induced GR hyperactivation may disrupt mitochondrial quality surveillance, potentially leading to enhanced autophagic clearance that involves mitochondria. Whether such excessive autophagic activity overwhelms mitochondrial biogenesis and ultimately contributes to RPE cell dysfunction remains a hypothesis that warrants further investigation.

Our experimental data demonstrate that GC exposure is associated with changes in the AMPK/mTOR pathway in RPE cells, as indicated by increased p-AMPK, decreased p-mTOR, and elevated LC3-II levels. This pathway is a well-established regulatory hub for autophagy, wherein p-AMPK is considered an upstream signal[30]. Mechanistically, AMPK can be involved in autophagy initiation either by directly phosphorylating Unc-51-like autophagy activating kinase 1 (ULK1) or by relieving mTOR complex 1 (mTORC1)-mediated inhibition of ULK1; subsequent ULK1 activation drives autophagosome formation, whereas mTORC1 constitutively suppresses this process *via* phosphorylation of autophagy-related gene 13 (ATG13)[31-32]. Consistent with the involvement of this pathway in RPE homeostasis, Yang *et al*[18] reported that Sirt3 attenuates high glucose-induced RPE injury and mitophagy

by modulating AMPK/mTOR/ULK1 signaling. Accordingly, our findings suggest that GC-induced alterations in the AMPK/mTOR pathway are associated with increased autophagic activity in RPE cells, including features suggestive of mitochondrial involvement.

While this study offers *in vitro* mechanistic insights into GC-induced RPE injury, several limitations should be acknowledged. First, the ARPE-19 monoculture model lacks key physiological components such as choroidal vasculature and RPE-photoreceptor interactions; moreover, immortalized cell lines may not fully recapitulate the behavior of primary RPE cells. Second, the GC concentrations used here may not accurately reflect the spatiotemporal dynamics of endogenous cortisol exposure in human CSC pathogenesis. Third, our autophagy readouts (LC3-II accumulation and mCherry-GFP-LC3B flux) are not specific to mitophagy; therefore, we interpret our data as autophagic flux with ultrastructural evidence suggestive of mitochondria-targeted autophagy. Fourth, although our pharmacological inhibition confirms GR dependence, rescue experiments targeting downstream pathways, such as through autophagy inhibition or AMPK/mTOR modulation, would be needed to further establish causality. Finally, all findings are derived from *in vitro* experiments; future validation using *in vivo* models, such as mice subjected to systemic GC exposure, will be important to determine whether excessive autophagic activity (with potential mitochondrial involvement) contributes to RPE pathology in a physiologically integrated context.

This study suggests that, in ARPE-19 cells, GC-induced mitochondrial GR accumulation is associated with autophagy involving mitochondria and changes in the AMPK/mTOR pathway, correlating with RPE barrier disruption and phagocytic failure, features of CSC-associated RPE dysfunction. These *in vitro* findings indicate a possible link between GC exposure and steroid-associated CSC.

ACKNOWLEDGEMENTS

Authors' Contributions: Guan WX and Guo Y contributed equally to this work. Conceptualization and methodology were provided by Guan WX and Guo Y; Investigation and formal analysis were finished by Guan WX, Guo Y, Chen ST, Liu ZM, and Sun YY; Original draft was written by Guan WX and Guo Y; Revisions were done by Zhao MW and Sun YY; Daily supervision and project administration were provided by Zhao MW. All authors reviewed and approved the final version of the manuscript.

Data Availability Statement: All data produced in the present study are available upon reasonable request to the corresponding author.

AI-Generated Content Disclosure: The authors declare that no artificial intelligence (AI) tools or large language models were used in the writing, analysis, or generation of any content in this manuscript.

Foundation: Supported by the National Natural Science Foundation of China (No.82301211).

Conflicts of Interest: Guan WX, None; **Guo Y,** None; **Chen ST,** None; **Liu ZM,** None; **Sun YY,** None; **Zhao MW,** None.

REFERENCES

1 Fung AT, Yang Y, Kam AW. Central serous chorioretinopathy: a review. *Clin Exp Ophthalmol* 2023;51(3):243-270.

2 Feenstra HMA, van Dijk EHC, Cheung CMG, *et al*. Central serous chorioretinopathy: an evidence-based treatment guideline. *Prog Retin Eye Res* 2024;101:101236.

3 You EL, Hébert M, Jin TS, *et al*. Comparing interventions for chronic central serous chorioretinopathy: a network meta-analysis. *Surv Ophthalmol* 2023;68(4):601-614.

4 Liu YC, Wu B, Wang Y, *et al*. Detection of macular ganglion cell complex loss and correlation with choroidal thickness in chronic and recurrent central serous chorioretinopathy. *Int J Ophthalmol* 2023;16(4):579-588.

5 Kaye R, Chandra S, Sheth J, *et al*. Central serous chorioretinopathy: an update on risk factors, pathophysiology and imaging modalities. *Prog Retin Eye Res* 2020;79:100865.

6 Nicholson BP, Atchison E, Ali Idris A, *et al*. Central serous chorioretinopathy and glucocorticoids: an update on evidence for association. *Surv Ophthalmol* 2018;63(1):1-8.

7 Brinks J, van Haalen FM, van Rijssen TJ, *et al*. Central serous chorioretinopathy in active endogenous Cushing's syndrome. *Sci Rep* 2021;11(1):2748.

8 Ge G, Zhang Y, Zhang YC, *et al*. Corticosteroids usage and central serous chorioretinopathy: a meta-analysis. *Graefes Arch Clin Exp Ophthalmol* 2020;258(1):71-77.

9 Leclercq B, Weiner A, Zola M, *et al*. The choroidal nervous system: a link between mineralocorticoid receptor and pachychoroid. *Acta Neuropathol* 2023;146(5):747-766.

10 Sesar A, Sesar AP, Jurisic D, *et al*. Unraveling the puzzle of central serous chorioretinopathy: exploring psychological factors and pathophysiological mechanisms. *Med Sci Monit* 2023;29:e941216.

11 Liu SZ, Yao SJ, Yang H, *et al*. Autophagy: regulator of cell death. *Cell Death Dis* 2023;14(10):648.

12 Liu J, Liu Y, Wang Y, *et al*. TMEM164 is a new determinant of autophagy-dependent ferroptosis. *Autophagy* 2023;19(3):945-956.

13 Ajoolabady A, Wang SY, Kroemer G, *et al*. Targeting autophagy in ischemic stroke: from molecular mechanisms to clinical therapeutics. *Pharmacol Ther* 2021;225:107848.

14 Lu YY, Li ZJ, Zhang SQ, *et al*. Cellular mitophagy: mechanism, roles in diseases and small molecule pharmacological regulation. *Theranostics* 2023;13(2):736-766.

15 Wang J, Zhang Y, Cao J, *et al*. The role of autophagy in bone metabolism and clinical significance. *Autophagy* 2023;19(9):2409-2427.

16 Deng JL, Guo YJ, Yuan FX, *et al*. Autophagy inhibition prevents glucocorticoid-increased adiposity *via* suppressing BAT whitening. *Autophagy* 2020;16(3):451-465.

17 Kokkinopoulou I, Moutsatsou P. Mitochondrial glucocorticoid receptors and their actions. *Int J Mol Sci* 2021;22(11):6054.

18 Yang W, Qiu C, Lv HB, *et al*. Sirt3 protects retinal pigment epithelial cells from high glucose-induced injury by promoting mitophagy through the AMPK/mTOR/ULK1 pathway. *Transl Vis Sci Technol* 2024;13(3):19.

19 Datta S, Cano M, Satyanarayana G, *et al*. Mitophagy initiates retrograde mitochondrial-nuclear signaling to guide retinal pigment cell heterogeneity. *Autophagy* 2023;19(3):966-983.

20 Zhang ZQ, Xie Z, Chen SY, *et al*. Mitochondrial dysfunction in glaucomatous degeneration. *Int J Ophthalmol* 2023;16(5):811-823.

21 Jiang S, Li HQ, Zhang L, *et al*. Generic Diagramming Platform (GDP): a comprehensive database of high-quality biomedical graphics. *Nucleic Acids Res* 2025;53(D1):D1670-D1676.

22 Timmermans S, Souffriau J, Libert C. A general introduction to glucocorticoid biology. *Front Immunol* 2019;10:1545.

23 Kadmiel M, Cidlowski JA. Glucocorticoid receptor signaling in health and disease. *Trends Pharmacol Sci* 2013;34(9):518-530.

24 Li ZY, Li QZ, Chen L, *et al*. HPOB, an HDAC6 inhibitor, attenuates corticosterone-induced injury in rat adrenal pheochromocytoma PC12 cells by inhibiting mitochondrial GR translocation and the intrinsic apoptosis pathway. *Neurochem Int* 2016;99:239-251.

25 Du J, Wang Y, Hunter R, *et al*. Dynamic regulation of mitochondrial function by glucocorticoids. *Proc Natl Acad Sci U S A* 2009;106(9):3543-3548.

26 Choi GE, Han HJ. Glucocorticoid impairs mitochondrial quality control in neurons. *Neurobiol Dis* 2021;152:105301.

27 Zhou R, Li JJ, Zhang L, *et al*. Role of Parkin-mediated mitophagy in glucocorticoid-induced cardiomyocyte maturation. *Life Sci* 2020;255:117817.

28 Yuan J, Gao YS, Liu DL, *et al*. PINK1-mediated mitophagy contributes to glucocorticoid-induced cathepsin K production in osteocytes. *J Orthop Transl* 2023;38:229-240.

29 Chen KY, Chan HC, Lin WW, *et al*. Mitochondrial dynamics and their role in the pathogenesis of age-related macular degeneration: a comprehensive review. *Redox Bio* 2026;93:103976.

30 Kim J, Kundu M, Viollet B, *et al*. AMPK and mTOR regulate autophagy through direct phosphorylation of Ulk1. *Nat Cell Biol* 2011;13(2):132-141.

31 Kim YC, Guan KL. mTOR: a pharmacologic target for autophagy regulation. *J Clin Invest* 2015;125(1):25-32.

32 Huang JS, Chen ZX, Wu ZY, *et al*. Geniposide stimulates autophagy by activating the GLP-1R/AMPK/mTOR signaling in osteoarthritis chondrocytes. *Biomed Pharmacother* 2023;167:115595.